The Berkeley High Resolution Tropospheric NO_2 Product

Response to Anonymous Referee #2

Joshua L. Laughner, Qindan Zhu, and Ronald C. Cohen

September 11, 2018

We thank the reviewer for their careful reading and especially their critical thinking about the explanation of the difference between average VCDs using daily and monthly profiles and our explanation of the root cause for the difference between the new and old visible AMF formulation. We have reexamined our conclusions in both cases and made edits where appropriate.

Responses to specific comments follow. The reviewer's comments will be shown in red, our response in blue, and changes made to the paper are shown in black block quotes. Unless otherwise indicated, page and line numbers correspond to the original paper. Figures, tables, or equations referenced as "Rn" are numbered within this response; if these are used in the changes to the paper, they will be replaced with the proper number in the final paper. Figures, tables, and equations numbered normally refer to the numbers in the original discussion paper.

However, I have got the feeling, at least from the abstract, that the manuscript is more suitable to journals like AMT or ACP, since it is mainly talking about algorithm instead of the dataset itself. Therefore, I would suggest the authors to update the abstract and maybe also the conclusion with more descriptions about the dataset...

Because the BEHR product will continue to evolve as we learn more about the ideal design of high-resolution NO_2 retrievals, we believe that ESSD's living data process is an ideal way to communicate those updates. For a satellite NO_2 product, where the assumptions and a priori data about the atmosphere can have a significant impact on the final NO_2 VCDs, we feel that it is important to show how the evolution of these assumptions impacts the VCDs. Nevertheless, this is a fair comment, as we also have a responsibility to describe the dataset for the users. To this end, we have expanded both the section on usage recommendations, to give users some guidance on typical uses for BEHR data, and added more information about the primary variables in the Appendix:

"

General recommendations

Quality filtering

It is vital in any use of BEHR data to filter out low quality data. The BEHR algorithm attempts to calculate an NO_2 VCD for as many pixels as possible, even if some of those pixels are known to be poor quality. The philosophy is that it is better to have data for a pixel if at all possible and remove it only if the quality is too low for a particular application. Some causes of low quality (e.g. the row anomaly, `https://projects.knmi.nl/omi/research/product/rowanomaly-background.php`) make the NO_2 column unusable under any case, while others (e.g. high cloud fraction, low quality surface reflectance) only affect certain uses.

The quality of the pixel is summarized in the first two (least-significant) bits of the BEHRQualityFlags field. The second bit is a critical error bit, if set (i.e. if a bitwise AND of BEHRQualityFlags with 2 is > 0) then the NO_2 columns for that pixel should not be used under any conditions. The first bit is a quality flag bit; if it is set (if a bitwise AND of BEHRQualityFlags with 1 is > 0) then the use of the column for typical applications wanting information down to the surface is not recommended; however, other applications may still find use for this pixel. For example, the first bit is set if the OMI geometric cloud fraction is > 0.2, since the uncertainty of the total tropospheric column increases greatly as more NO_2 is obscured by clouds, but cloud slicing approaches (e.g. Choi et al., 2014; Marais et al., 2018) will actually prefer large cloud fractions, and so will need to do their own cloud filtering. For most applications however, it is recommended to ignore pixels that have the first (i.e. quality summary) bit set to 1.

Users must also be sure to remove fill values. The fill value for each field is defined in the "fillvalue" attribute. Generally, checking if a value is exactly equal to a fill value is not recommended unless the value is an integer type, as floating point error on some systems may cause fill values to be missed. It is better practice to check for values within some relative tolerance of the fill value:

$$|x - f| < |f| \cdot t \tag{R1}$$

where x is the data, f is the fill value, and t the tolerance. $t = 10^{-4}$ works in our experience.

Choice of daily or monthly profile subproduct

Users will also need to choose whether to use the subproduct with daily profiles. Use of the subproduct with daily profiles is strongly encouraged if possible, for two reasons. First, the daily profiles also use year specific emissions (Sect. 2.6.1, so will better capture trends in VCDs as the surface contribution to the a priori profiles is reduced. Second, Laughner et al. (2016) showed that using daily profiles

significantly changes day-to-day VCDs, and that some applications of satellite data can be biased when monthly profiles are used. Applications similar to those studied in Laughner et al. (2016), where upwind or downwind columns are systematically averaged together are particularly vulnerable to bias when monthly average profiles are used.

Caution is advised if comparing 2005 or 2006 data using daily profiles to other years; the different WRF-Chem boundary conditions (Sect. 2.6.1) may also bias observed trends. This effect is likely small, as in a test of 1 week of data using two sets of profiles, one using GEOS-Chem boundary conditions and one using MOZART boundary conditions, the mean change was $< 10^{14}$ molec cm^{-2}, and only 0.7% of pixels with any cloud fraction had a change exceeding 10^{15} molec cm^{-2} (0.05% of pixels with cloud fraction < 0.2).

However, mixing daily and monthly profile subproducts is *strongly* discouraged, as systematic differences between them (i.e. Sect. 4.3.2 of this paper; Laughner et al., 2016) will bias any trends observed.

Application #1: direct observation of VCDs

Direct observation of VCDs has a number of applications, including elucidating trends in NO_2 burdens (e.g. Russell et al., 2012; Jiang et al., 2018) or inferring lightning emissions (e.g. Pickering et al., 2016). Users wanting to average BEHR data over a given time period, e.g. to compare summer average NO_2 columns for different years, will find this easiest using the gridded data, as this places the NO_2 columns on a consistent equirectangular latitude/longitude grid (i.e. the data in grid cell (1,1) will be at the same lat/lon in each orbit, whereas in the native data, pixel (1,1) will not), so it is easy to average across different days. When averaging, each grid cell should be weighted by the Areaweight value given in the gridded product; this is the inverse of the pixel area, so weighting by this inherently gives more weight to smaller, more representative pixels.

Users interested in VCDs from individual days (e.g. to find NO_2 downwind of an episodic event such as lightning) can use either the native pixel or gridded products, whichever is easier. In this case, it is important to keep in mind that pixel sizes vary from day-to-day. Therefore, if the source signal of interest is smaller than a single pixel, it will be more diluted if it falls in a larger pixel on the edge of the OMI swath than a small one near the center.

Application #2: inferring surface NO_2 concentration

Since a VCD is a measurement integrated over the troposphere, it does not directly provide information about the surface concentration of NO_2. The simplest approach to infer ground-level NO_2 concentrations from VCDs is to multiply the BEHR VCD by the ratio of surface concentration to VCD obtained from a modeled NO_2 profile (Lamsal et al., 2008):

$$[\mathrm{NO_2}]_{\mathrm{surf}} = \frac{g(p_{\mathrm{surf}})}{\int_{p_{\mathrm{surf}}}^{p_{\mathrm{trop}}} g(p)\, dp} V_{\mathrm{BEHR}} \tag{R2}$$

where $g(p)$ is the modeled profile, p_{surf} the surface press, p_{trop} the tropopause pressure, and V_{BEHR} the BEHR VCD. $g(p)$ may be obtained in many ways; for users without model output or measurements of $\mathrm{NO_2}$ profiles, the a priori profiles used in BEHR are included in the native pixel subproduct and may be used for this purpose. In this case, using the subproduct with daily profiles is highly recommended so that the profiles respond to changes in meterology day to day, especially wind fields.

Application #3: comparing to models

Users wishing to compare BEHR VCDs to model output should follow the suggestions in Boersma et al. (2016). This requires calculating the overlap between the BEHR pixels and the user's model grid cells and applying the BEHR averaging kernel to the user's model profile before calculating the model VCD, so the native pixel product must be used, since it contains the averaging kernels and the pixel corners.

The averaging kernels would be applied to the model profile as:

$$V_{\mathrm{model}} = \sum_k c_k a_k \tag{R3}$$

where V_{model} is the modeled VCD after applying the averaging kernels, k is the level index, c_k is the model profile converted to a partial column for level k, and a_k is the averaging kernel for level k.

There are three important considerations in this application. First, since BEHR provides only a tropospheric VCD, it must be compared against a modeled tropospheric column, no stratospheric component may be included.

Second, the model $\mathrm{NO_2}$ profile should be interpolated to the pressure levels on which the averaging kernels are defined (given in the BEHR files as BEHRPressureLevels) rather than the other way around. This is because the averaging kernels may have sharp changes between levels (usually at the cloud pressure, since OMI's sensitivity increases dramatically over a bright cloud) so interpolating the averaging kernels to the model pressures is more likely to introduce errors.

Third, the model profile is best converted to partial columns before applying the averaging kernels. This may be done several ways, such as:

- Interpolate the profile to the averaging kernels' pressure levels, then multiply the profile concentration as number density by the layer height.

- Interpolate the profile to the *edges* of the averaging kernels' levels, then integrate over each layer to obtain the partial column.

Both methods need the edge of the pressure levels, either to calculate the box height or to define the limits of the integration. Since the pressures given for the averaging kernels are the level centers, the edges are most easily defined as the midpoints between those layers; with the surface pressure serving as the lower limit of the bottom layer and the tropopause pressure serving as the upper limit of the top layer.

Converting from pressure to altitude for either method can either be done using a scale height relation (e.g. Eq. 10), though this will likely introduce some error as we saw in Sect. 5.4 that the meteorological correction can be significant. A better option, if the user's model output includes altitude and pressure vectors, is to interpolate the altitude from the model to the averaging kernels' pressure levels alongside the NO_2. Alternatively, in the second method, NO_2 profiles in mixing ratio can be directly integrated over pressure (Ziemke et al., 2001, Appendix B). This is done internally in BEHR using the integPr2 code at `https://github.com/CohenBerkeleyLab/BEHR-core-utils/blob/develop/AMF_tools/integPr2.m`.

(Appendix) Key variables

The BEHR files contain a large number of variables, including a large amount of ancillary data used in the algorithm. All variables in the HDF files have a "description" attribute that provides some information about what they are. They also have a "product" attribute that indicates whether they are taken verbatim from the NASA Standard Product (product = "SP") or added by BEHR (product = "BEHR"). The primary variables that most users should focus on are:

- **BEHRColumnAmountNO2Trop**: This is the tropospheric VCD calculated using Eqs. (1) and (2). It is the concentration of NO_2 integrated from the surface to the tropopause, including NO_2 below clouds. This is the NO_2 value that most users should use.
- **BEHRColumnAmountNO2TropVisOnly**: This is the visible-only tropospheric VCD calculated with Eqs. (1) and (3). It excludes below-cloud NO_2. Generally the use for this quantity is more specialized; most users should use the previous value.
- **BEHRQualityFlags**: A 32-bit unsigned integer value where each bit represents a boolean flag indicating the presence of a specific error or warning for that pixel. See Sect. A3 for details.
- **Areaweight** (*gridded products only*): a weight calculated of the inverse of the area of the pixel that each grid cell falls within. This should be used to weight the gridded data during temporal averaging (see Sect. 7).
- **Longitude**, **Latitude**: the coordinates of the pixel or grid cell center.

- **CloudFraction**: this is a geometric cloud fraction from the OMI $O_2{-}O_2$ cloud product (Acarreta et al., 2004). It is the default used to filter for cloudy pixels, and is the same as the corresponding variable in the NASA Standard Product.
- **CloudRadianceFraction**: this is a radiance cloud fraction (i.e. one weighted by the amount of light coming from the cloud vs. the ground). It is the same as the corresponding field in the NASA Standard Product.
- **MODISCloud**: this is a geometric cloud fraction from the Aqua MODIS instrument (Platnick et al., 2015) averaged to the OMI pixels. It is an alternate way of filtering for cloudy pixels that may be less susceptible to false positives from highly reflective ground (Russell et al., 2011). Some pixels near the edge of the swath may be missing this data since the MODIS swath width is slightly smaller than OMI's.

More advanced users may find the 3D variables included in the native pixel subproducts useful. These variables give a unique vector of values for each pixel. In Matlab, the vector for each pixel runs along the first dimension, so if the NO_2 VCDs are the 2D array `V` and one of the 3D arrays is `A`, then the vector corresponding to `V(i,j)` would be `A(:,i,j)`. However, some languages reverse the order of the dimensions. In BEHR v3.0B, the vector dimension can be identified as the one with a length of 33.

In BEHR, these 3D variables are defined on a vertical grid of 30 standard pressure levels (ranging from 1020 to 60 hPa) with values interpolated to the surface pressure, cloud pressure, and tropopause pressure included, brining the total length of the vertical dimension to 33. If one of the interpolated pressure levels is the same as a standard pressure level, the value is not duplicated, and the vector of values will be padded with fill values at the end.

- **BEHRPressureLevels**: this dataset defines the pressure levels that the other 3D variables are defined on.
- **BEHRNO2apriori**: this dataset gives the NO_2 a priori profiles used in the BEHR retrieval in mixing ratio.
- **BEHRAvgKernels**: these are the averaging kernels referenced in Sect. 7.4. They are defined as:

$$a(p) = \frac{(1-f)w_{\text{clear}}(p)\alpha(p) + f w_{\text{cloudy}}(p)\alpha(p)}{A} \tag{R4}$$

  where $a(p)$ is the averaging kernel, f the cloud radiance fraction, $\alpha(p)$ the temperature correction (Eq. 6) and $w_{\text{clear}}(p)$ and $w_{\text{cloudy}}(p)$ the clear and cloudy scattering weights, which are set to 0 below the surface and cloud pressure, respectively.
- **BEHRScatteringWeightsClear**, **BEHRScatteringWeightsCloudy**: the temperature corrected clear and cloudy scattering weights, set to 0 below the surface and cloud pressure, respectively, i.e.:

$$w'_{\text{clear}}(p) = w_{\text{clear}}(p)\alpha(p) \quad \text{(R5)}$$
$$w'_{\text{cloudy}}(p) = w_{\text{cloudy}}(p)\alpha(p) \quad \text{(R6)}$$

”

general: Despite the good written language, the organization sometimes makes it difficult for me to identify which improvement is for v3.0A which is for v3.0B. For instance, in the “Methods” section, some methods are introduced for v3.0A and some are for v3.0B. Also, the methods of older version are sometimes introduced in “Methods” section (e.g. surface pressure) and sometimes in each subsection (e.g. visible-only AMF calculation). Therefore, this methods section is not fully referable when reading the following sections. In addition, illustrations like “figure 1 shows...” and “table 1 shows...” are missing.

We have added references to figures and tables in the relevant sections. Most notably, the main figures (1 and 4 in the discussion paper) are introduced in a new “Paper structure” section that comes before the detailed analysis of the results.

> “In sections 4 and 5, we evaluate the effect each change to the BEHR algorithm between v2.1C and v3.0B had on the tropospheric VCDs. In order to provide a clear history, changes introduced in v3.0A will be discussed first (Sect. 4), followed by changes introduced in v3.0B (Sect. 5). V3.0A incorporated all changes up through the introduction of the new gridding algorithm; the remainder are added in v3.0B. Changes to the visible-only VCDs (i.e. those excluding the below-cloud column) are discussed in the supplement (Sect. S1). Following this the overall difference between v2.1C and v3.0B will be presented in Sect. 6. Recommendations for the use of the product are given in Sect. 7. A description of the data format is given in Appendix A.
>
> For the discussion of how changes to the algorithm affect the NO_2 VCDs, figures 1 and 2 and Tables 3 and 4 are the central focus. Each panel shows the change in the BEHR NO_2 VCDs resulting from a specific change to the algorithm. To generate these figures, BEHR VCDs were computed after adding each change to the algorithm incrementally. Each panel in the figures and line in the tables shows the percent change in VCDs due to the corresponding change to the algorithm. These are computed relative to VCDs with one fewer change to the algorithm; for example, Fig. 1b is the percent difference between VCDs using the new NASA SCDs and the new MODIS BRF surface reflectance versus VCDs using just the new NASA SCDs. The (a) panels in Figs. 1 and 2 and the first lines in Tables 3 and 4 are relative to BEHR v2.1C.
>
> Figure 1 shows the percent change of average BEHR tropospheric VCDs due to each algorithm improvement for the subproduct using monthly average NO_2 a priori profiles, while Fig. 2 shows the changes to the subproduct using daily NO_2 a priori profiles. (Figure 2 has fewer panels than Fig. 1 as daily profiles were only possible in increments after the change to the algorithm to introduce the new a

Component	v3.0A	v3.0B	Section
Ocean reflectance	Calc. for 430 nm	Calc. for 460 nm	2.2
Surface pressure	Scale height	WRF pressure adjusted with GLOBE elevation	2.3
Tropopause pressure	Fixed at 200 hPa	Calculated from WRF temperature profiles	2.4
Daily prof. hour	Last hour before overpass	Closest hour to overpass	2.6.2

Table R1: Summary of differences in methods between v3.0A and v3.0B.

priori profiles was implemented.) Both figures are for summer (June–Aug.) 2012. Winter changes are presented in the supplement.

Table 3 gives the mean and median changes for each incremental improvement shown in Figs. 1 and 2; that is, it gives the domain-wide mean and median values of the time-averaged changes shown in the figures. Table 4 is similar, but is the statistics for individual pixels, rather than the time-averaged changes."

For the methods section, we have generally edited it to make clear which methods are applicable to v3.0A and which to v3.0B, including a summary table:

The visible-only AMF given in the methods is the only form used in both v3.0A and v3.0B, so including the old form in the methods for v3.0x might add confusion. We have added a sentence referring the reader to the appropriate section:

"Replacing A_{BEHR} in Eq. (1) with $A_{\mathrm{BEHR,vis}}$ yields a visible-only NO_2 column as the output, stored in the variable "BEHRColumnAmountNO2TropVisOnly" in the BEHR files. **The form of this visible AMF changed from v2.1C to v3.0A; please see Sect. S1 in the Supplement for details of the old calculation.**"

""

page2line4 GOME2 (GOME2A in 2006 and GOME2B in 2012) is newer than OMI.

We have removed GOME2 from this sentence:

"The spatial resolution available with early instruments (i.e. the Global Ozone Monitoring Experiment, GOME, 40×320 km^2, Burrows et al. 1999b; the SCanning Imaging Absorption SpectroMeter for Atmospheric CHartographY, SCIAMACHY, 30×60 km^2, Noel et al. 1998) allowed inferences at the scale of entire continents or entire metropolitan regions..."

page2line24 I believe the difficulty of NO observation is not only because of the absorption in UV. Even it is noisier than VIS, it still works for gases, e.g. O3 and even possible for NO2. Please specify this sentence.

We believe that the difficulty in measuring tropospheric NO specifically is that the absorbance features overlap with the strong ozone absorption band, so NO absorption in the troposphere is obscured. However, we have not found any citations that explicitly state this, so for simplicity we have altered this to just note that NO is not measured by any sensors currently in orbit:

"The current fleet of space-based sensors measures NO_2, not total NO_x, but due to the rapid daytime equilibrium between NO and NO_2, this allows inferences about tropospheric NO_x to be made from NO_2 measurements."

page2line25 "inferences about total NOx are made from NO2 measurements" maybe also because of the quick conversion of NO to NO2?
We have added:

"In contrast, NO_2 has useful absorbance in the visible wavelengths, outside the strong ozone absorption band. In combination with the rapid daytime equilibrium between NO and NO_2, this allows inferences about tropospheric NO_x to be made from NO_2 measurements."

page3line4 I suggest including the TM5 also as examples, since it is largely used currently, e.g. for OMI and TROPOMI retrieval.
We have added TM5 to this list.

page3line3-11 I recommend combining these two paragraphs together, since they both talk about how to calculate AMFs, and the "input data" in line 12 talks mainly about the input data (i.e. profiles) in the 1st paragraph.
We have combined these two paragraphs as suggested.

page5line8 The definition of RRA it not that special, can be removed.
We have found that different communities use different conventions for RAA; some define 0 as the sun and viewer are on the same side, others define it as the sun and viewer are directly opposite each other. We prefer to be explicit about how we define RAA so there is no confusion, and this seems the logical place to do so.

page6line10 What does "BEHR uses the file dated for the day being retrieved for the BRF coefficients." mean?
We have clarified this with an example:

"BEHR uses the file dated for the day being retrieved for the BRF coefficients, **i.e. for 1 June 2012, the MODIS files with 1 June 2012 in the file name are used. This means that the surface reflectivity used in BEHR incorporates land data from 8 days before and after the OMI observation.**"

page8line7 Why does the BEHR include these different cloud products? For instance, is there a specific reason to include MODIS cloud fraction? Please also add more information about the OMI-derived quantities. Do you retrieve the cloud fractions, or do you use OMCLDO2 or OMCLDRR?
We have added:

"BEHR contains several cloud fraction products: **a geometric cloud fraction derived from the O_2-O_2 algorithm (Acarreta et al., 2004), a cloud radiance fraction calculated by NASA from the O_2-O_2 product,** and a geometric cloud fraction derived from the Aqua MODIS instrument, and cloud pressure from the OMI O_2-O_2 algorithm (Acarreta et al., 2004). The OMI-derived quantities are the same as those in the NASA SP v3.0. The MODIS cloud product used is MYD06_L2 (Platnick et al., 2015).

Russell et al. (2011) found that the MODIS cloud product was less likely to give erroneously large cloud fractions due to high surface reflectivity over the California and Nevada desert, and concluded that this more than offset any error caused by the small separation between the overpass times (currently $\sim$ 8 min) of OMI on board the Aura satellite and MODIS on board the Aqua satellite. We continue to provide the MODIS cloud product for cloud filtering; however, because it does not cover the full OMI swath, we use the OMI cloud fractions in the AMF calculations."

Also, please update the expression "radiance cloud fraction" to cloud radiance fraction here and through the manuscript.

So updated.

page8line28 What output is used here?

The chemical concentrations are used for WRF-Chem boundary conditions. We have clarified as:

"**Chemical boundary conditions for WRF-Chem are taken two different global models.** For model years 2007 and later, **chemical concentrations** from the Model for Ozone and Related chemical Tracers (MOZART, Emmons et al., 2010) provided by the National Center for Atmospheric Research"

page9line7 When would this extrapolation happen? If it is because of the different surface pressure from scattering weight and profiles, then it might be even better to shift the profile but not extrapolate.

Yes, this happens if the surface pressure of the pixel is below the bottom of the profile. Shifting the profile is an interesting idea, though if large shifts were required, it could possibly introduce different errors by e.g. placing the boundary layer or upper tropospheric lightning at the wrong altitudes. One thing we had not mentioned originally is that the extrapolation is only allowed to extend the profile by one pressure level. Near the surface the pressure levels are quite close together (5 hPa) and even at 1 km elevation the spacing is only 25 hPa, so we expect the error to be minimal. We have added text describing this:

"**The profiles are also extrapolated to one scattering weight pressure level above and below the top and bottom of the WRF profile, respectively. This accounts for the possibility that e.g. a pixel's surface**

pressure may be slightly below the WRF surface pressure, but by limiting the extrapolation to only one level, should minimize errors due to extrapolation. Once interpolated and extrapolated, all profiles within the..."

page9line14 Please specify "when possible".
Changed to:

"We make use of daily profiles **for as much of the OMI data record as it is computationally feasible to simulate these profiles.** "

page11table2 What is ocean LUT here and through the manuscript? Do you mean ocean reflectance LUT?
Yes, we have clarified this in the caption and elsewhere.

page11figure2 This figure is comparing with BEHR v3.0B but it is described in the "Changes in BEHR v3.0A" text. Additionally, the interpretation after figure is talking about the changes in surface reflectance over land. Please add more analysis about changes over water, since the difference is quite significant.
We have made the comparison with v3.0A instead. We also incorporated the decomposition of changes due to the change of MODIS version vs. black-sky to BRF in response to a comment from the first reviewer, as well as added a panel showing the ocean LUT and added the following text:

"

BEHR v2.1C used an ocean reflectance look-up table embedded in the core code that defined how the dependence of the ocean reflectance on solar zenith angle (SZA). As documentation of the source for this table is not available, BEHR v3.0A switched to a new look up table calculated explicitly using the Coupled Ocean-Atmosphere Radiative Transfer (COART) model (Jin et al., 2006). The difference in the SZA dependence of the look up tables is shown in Fig. 3g. The overall shape is similar, but the difference between small and large SZAs is less pronounced in the new ocean look-up table. Both are similar to the ocean surface reflectance calculated by Jin et al. (2004) for an atmospheric aerosol optical depth of 1, but for different wind speeds: the BEHR v2.1C look-up table is more characteristic of slow (< 1 m s^{-1}) winds, while the v3.0A table assumes a wind speed of 5 m s^{-1}.

At small SZAs characteristic of summer OMI observations ($< 35°$), the new look up table yields a $\sim$ 50% greater ocean reflectance than the old table, which leads to the off-shore reflectance changes seen in Fig. 3a. At larger SZAs more characteristic of winter ($\sim 40°$ to $60°$), the difference between the old and new look-up tables shrinks, resulting in less change in the wintertime ocean surface reflectance (Fig. 3d).

Especially in summer, since the relative change in the ocean surface reflectance is large, using the new ocean look-up table does result in large relative changes

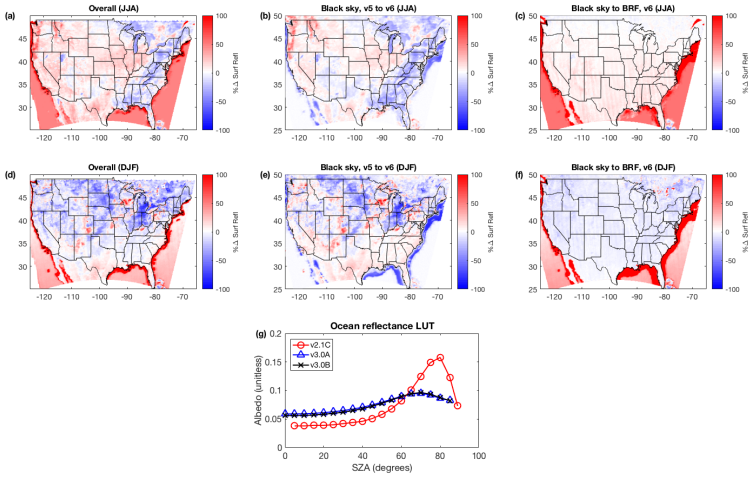

Figure R1: (a,d) Difference in surface reflectance between BEHR v2.1C (MODIS MCD43C3 black sky albedo, old ocean look up table) and BEHR v3.0B (MODIS MCD43Dxx BRF, new look up table) (b,e) Difference in surface reflectance between version 5 and 6 of the MODIS black sky albedo (no change in ocean look up table). (c,f) Difference in surface reflectance between the MODIS black sky and BRF product and the change in ocean look up table. (a–c) are for summer (JJA) and (d–f) are for winter (DJF). (g) The ocean albedo look-up table values for v2.1C, v3.0A, and v3.0B. (The change between v3.0A and v3.0B is discussed in Sect. 5.2.)

to the NO_2 VCDs. Along the coasts, these changes can reach 2×10^{15} to 3×10^{15} molec cm^{-2} (or more near New York, NY), but away from the coasts, the absoluate differences are quite small."

page13figure3 The figures are not clear and the conclusions are not convincing to me. Why is there a straight line (a deep blue line with no percent change in NO2 near cloud pressure 700 hPa in (a) and a distinct line near the black dashed line in (b))? What is the definition of surface NO2 concentration and why does it matter here? Since in Eq. 2, it is only the profile shape (relative vertical distribution) matters in the AMF cal- culation but not the absolute concentration. Also, I am not sure with "Greater percent difference with greater surface NO2 concentration.", because most of the largest differ- ences in the figure are found for low surface NO2 concentration (blue to deep blue in (a)). Similarly, greater percent differences are also found for small difference between the cloud fraction and cloud radiance fraction, since quite a lot of yellow dots are close to the black dashed line in (b).

We have reevaluated our conclusions here. We have revised this section and updated the figure. The line near the black dashed line in the original (b) panel was caused by pixels that had a high surface reflectivity in the NASA product (~ 0.55), since when the ground is highly reflective, that reduces the discrepancy in light coming from the cloud vs. the ground, and so shrinks the difference between the geometric and radiance cloud fractions. Also please note that this section has been moved to the supplement, as in responding to a comment from Reviewer 1 we decided that the paper was more logically structured by including only the changes that impact the total tropospheric VCDs in the body of the main paper.

"As described in the methods (Sect. 2.1), BEHR has, since v2.1C, included both a total tropospheric NO_2 column and a "visible-only" column. Figure S1 provides a graphic definition of these terms. The visible-only column includes the NO_2 that would be visible if observing the pixel from directly above: for the cloudless part of the pixel, the column extends to the ground, but for the cloud covered part it only extends down to the cloud top. In contrast the standard total tropospheric column is the sum of the visible-only column and the ghost column, where the ghost column is the NO_2 below the clouds.

The AMF necessary to convert the observed slant columns to a visible-only vertical column (a what we will term a "visible-only" AMF) can be conceptualized two different ways. The formula for the v3.0 visible-only AMF is given in Eq. (3). Conceptually, this is the model SCD divided by the modeled VCD. In v2.1C, an alternate formulation was used:

$$A_{\text{BEHR,vis}} = (1 - f)A_{\text{clear,vis}} + fA_{\text{cloudy,vis}} \tag{R7}$$

where f is again the cloud radiance fraction and

$$A_{\text{clear,vis}} = \frac{\int_{p_{\text{surf}}}^{p_{\text{trop}}} w_{\text{clear}}(p) g(p)\, dp}{\int_{p_{\text{surf}}}^{p_{\text{trop}}} g(p)\, dp} \tag{R8}$$

$$A_{\text{cloudy,vis}} = \frac{\int_{p_{\text{cloud}}}^{p_{\text{trop}}} w_{\text{cloudy}}(p) g(p)\, dp}{\int_{p_{\text{cloud}}}^{p_{\text{trop}}} g(p)\, dp} \tag{R9}$$

This earlier method assumes that each pixel can be treated as two totally independent subpixels, one clear and one cloudy. This seems a logical extension of the independent pixel approximation (Cahalan et al., 1994; Marshak et al., 1998), but the physical interpretation is less clear than the new formulation.

Although both approaches to calculating a visible-only AMF (i.e. Eq. R7 and Eq. 3) are conceptually valid , they are not mathematically identical, and so the retrieved visible tropospheric NO_2 column increases between v2.1C and v3.0A Figure S2 shows the average change in visible-only NO_2 columns when changing from the v2.1C AMF to the v3.0A AMF. In the summer (Fig. S2a) the average increase approaches 100% over the eastern US, decreasing to 0 towards the west coast. In the winter (Fig. S2b) the difference is more sporadic.

The main cause for the change is the difference in how the relative magnitude of the NO_2 to-ground VCD and the above-cloud VCD is treated by the AMF calculation. In the v2.1C visible-only AMF formulation, the relative contribution of the clear- and cloudy- sky AMFs was entirely determined by the cloud radiance fraction. Equation (R7) can be written as:

$$A_{\text{BEHR,vis}} = (1 - f)\frac{S_{\text{clear}}}{V_{\text{clear}}} + f\frac{S_{\text{cloudy}}}{V_{\text{cloudy}}} \tag{R10}$$

where f is the cloud radiance fraction, S_{clear} and V_{clear} are the modeled slant and vertical NO_2 column density for the clear part of the pixel and S_{cloudy} and V_{cloudy} are likewise the modeled slant and vertical column density for the cloudy part of the pixel. V_{clear} and V_{cloudy} may be very different magnitudes (by a factor of up to 1000), especially in polluted areas where most of the NO_2 is near the surface and therefore below the cloud. However, the slant columns are related to their corresponding vertical columns through the scattering weights, which typically means the corresponding S and V values will be within about a factor of 2 or 3 of each other. This means that, in Eq. (R10), the relative magnitudes of $S_{\text{clear}}/V_{\text{clear}}$ versus $S_{\text{cloudy}}/V_{\text{cloudy}}$ will be similar, even if V_{clear} and V_{cloudy} (and likewise S_{clear} and S_{cloudy}) are substantially different.

In contrast, the new formulation could be written as:

$$A_{\text{BEHR,vis,new}} = \frac{(1 - f)S_{\text{clear}} + fS_{\text{cloudy}}}{(1 - f_g)V_{\text{clear}} + f_g V_{\text{cloudy}}} \tag{R11}$$

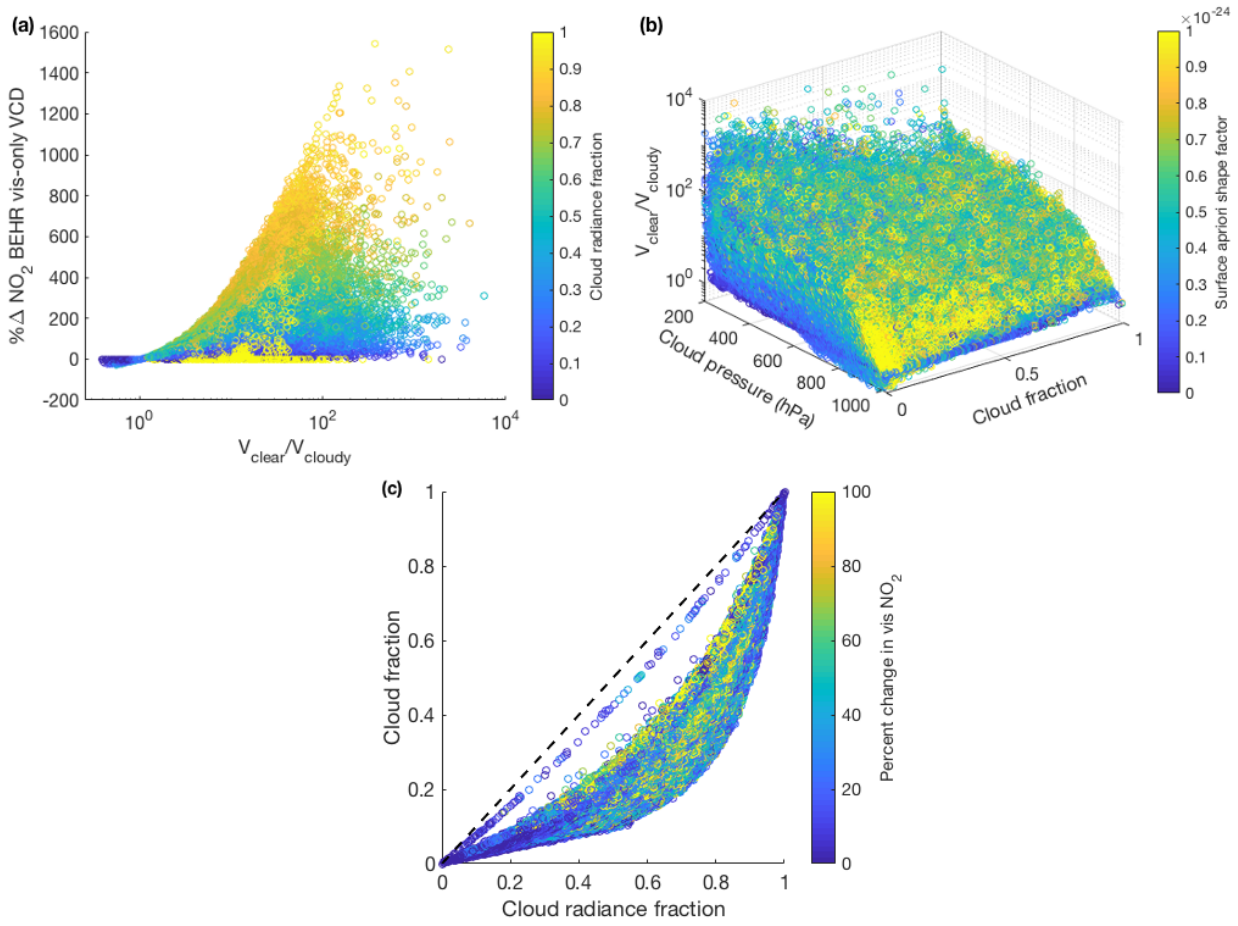

Figure R2: **(a)** The percent change in the visible-only BEHR NO_2 VCD versus the ratio modeled VCDs (V_{clear}, the WRF-Chem profiles integrated over the whole troposphere) to those integrated from cloud top to tropopause (V_{cloudy}), colored by cloud radiance fraction. **(b)** The ratio of $V_{\text{clear}}/V_{\text{cloudy}}$ versus geometric cloud fraction, cloud pressure, and colored by shape factor (mixing ratio/V_{clear}) at the surface. **(c)** The percent change in visible-only NO_2 VCD as a function of cloud radiance fraction and geometric cloud fraction. The black dashed line in (c) is the 1:1 line. *Note:* the color scale saturates at 10^{-24} in (b) and 100% in (c) to emphasize the distribution of the percent changes.

where f_g is the geometric cloud fraction. In this case, the relative magnitudes of S_{clear} versus S_{cloudy} and V_{clear} versus V_{cloudy} does matter. If $V_{\text{cloudy}} \ll V_{\text{clear}}$, then Eq. R11 reduces to

$$A_{\text{BEHR,vis,new}} = \frac{(1-f)S_{\text{clear}}}{(1-f_g)V_{\text{clear}}} \tag{R12}$$

whereas in Eq. (R10), the second term does not go to zero when $V_{\text{cloudy}} \ll V_{\text{clear}}$ because $S_{\text{cloudy}} \propto V_{\text{cloudy}}$. This means that, in theory, when $V_{\text{cloudy}} \ll V_{\text{clear}}$, the new visible-only AMF will essentially be a clear sky AMF, which will be less than a cloudy sky AMF since it includes near-surface NO_2 that OMI is less sensitive to. In contrast, in the old formulation, the relative contribution of the clear and cloudy components only depends on the cloud radiance fraction, not the relative magnitude of V_{clear} and V_{cloudy}, so the old visible-only AMFs will more often be of similar magnitude to a cloudy AMF. Because $V = S/A$ and $A_{\text{clear}} < A_{\text{cloudy}}$ in most cases, this means that the new visible-only NO_2 columns will be much larger than the old one.

In Fig. R2, we examine whether these effects show up in the BEHR data. Figure R2a shows the relative change in the visible-only NO_2 columns versus the ratio of $V_{\text{clear}}/V_{\text{cloudy}}$. The ratio $V_{\text{clear}}/V_{\text{cloudy}}$ sets a clear upper bound on the difference between the old and new visible-only NO_2 VCDs. What controls the ratio $V_{\text{clear}}/V_{\text{cloudy}}$ is shown in Fig. R2b. It increases rapidly as cloud pressure decreases, i.e. as the cloud hides more of the surface NO_2. When a large fraction of the NO_2 is near the surface, the effect is larger. This is illustrated by the fact that the top of the scatter in Fig. R2b has the greater surface NO_2 shape factor (here, the NO_2 mixing ratio divided by the column density). For a given cloud pressure, increasing the cloud fraction also increases $V_{\text{clear}}/V_{\text{cloudy}}$. All of these relationships are a natural result of clouds covering more NO_2.

In Fig. R2a, we also see that for a given ratio $V_{\text{clear}}/V_{\text{cloudy}}$, the magnitude of the difference between old and new BEHR NO_2 VCDs can vary quite significantly, depending primarily on the cloud radiance fraction. As the cloud radiance fraction decreases, the second term in both Eq. (R10) and Eq. (R11) becomes less important, so both become more similar to a clear-sky AMF and each other. However, at cloud radiance fractions near 1, the difference between old and new BEHR VCDs drops to 0. This happens because, as shown in Fig. R2c, when the cloud fractions are near 0 or 1, the geometric and radiance fractions converge, and for $f_g = f = 0$ or $f_g = f = 1$, Eq. (R10) and (R11) reduce to the same quantities.

To summarize, the conceptual difference is that the old AMF was a weighted sum of the clear and cloudy AMFs, but this did not account for the difference in magnitude between the to-ground and above cloud columns. The new AMF is a ratio of the expected slant column to the expected visible vertical column, which tends to include more NO_2 from the clear part of the pixel. Since OMI is

less sensitive overall to NO_2 in the clear part under most circumstances, the new AMFs are smaller, resulting in larger retrieved visible-only VCDs."

page14line21 What is UT?
Upper troposphere, we have defined it.

page15figure4 the (a) and (b) panels are not described anywhere.
We have added references in the appropriate sections (Sect. 4.3.2 and 4.4 respectively)

page15line3 I do not understand this hypothesis, since the profile shape itself depends not on the cloud information. The selection criteria of cloud fraction 0.2 only has impact on the NO2 column calculation, and it has no impact on the profile shape.

Our thinking was that, while the cloud fraction does not *directly* impact the profile shape, since clouds are correlated with lightning in the real world (and assuming that real world clouds correlated with modeled lightning), then selecting only cloud-free pixels would select for pixels whose daily profiles had less lightning contribution. In contrast, since the monthly profiles lack day-to-day variation, this would not affect them.

However, the first reviewer also found this section overly complex, so we have streamlined it, discussing only the actual conclusion: that the statistical distribution of UT NO_x concentrations propagates differently through the monthly and daily profiles.

"

Ultimately, the fact that lightning is an intermittent but significant NO_x source in the upper troposphere (UT) is the cause of this difference. Figure R3a shows the statistical distribution of NO_2 in the UT for two regions in the US: the southeast, which has significant lightning activity, and the northwest which has very little lightning. The distribution is highly skewed with a long tail in the southeast US due to the lightning activity, but not in the northwest US. Because of the nonlinear nature of the AMF calculation, this skewed distribution translates into different average VCD values.

Figure R3, panels b and c show average shape factors derived from monthly averaged and daily a priori profile for the southeast and northwest US. A shape factor is a profile divided by its integral:

$$S(p) = \frac{g(p)}{\int_{p_{\text{surf}}}^{p_{\text{trop}}} g(p)\, dp} \tag{R13}$$

A shape factor can be intepreted as the relative vertical distribution of NO_2. It appears implicitly in the AMF calculation (Eq. 2).

Here we see how the skewed UT NO_2 distribution affects the southeast US AMFs through the shape factor. Figure R3b shows that the statistically skewed UT NO_2 distribution causes shape factors calculated from the monthly average a priori profiles in the southeast US to have a larger fraction of the column NO_2 in the UT than that calculated from the daily profiles. Through Eq. (2), this leads to

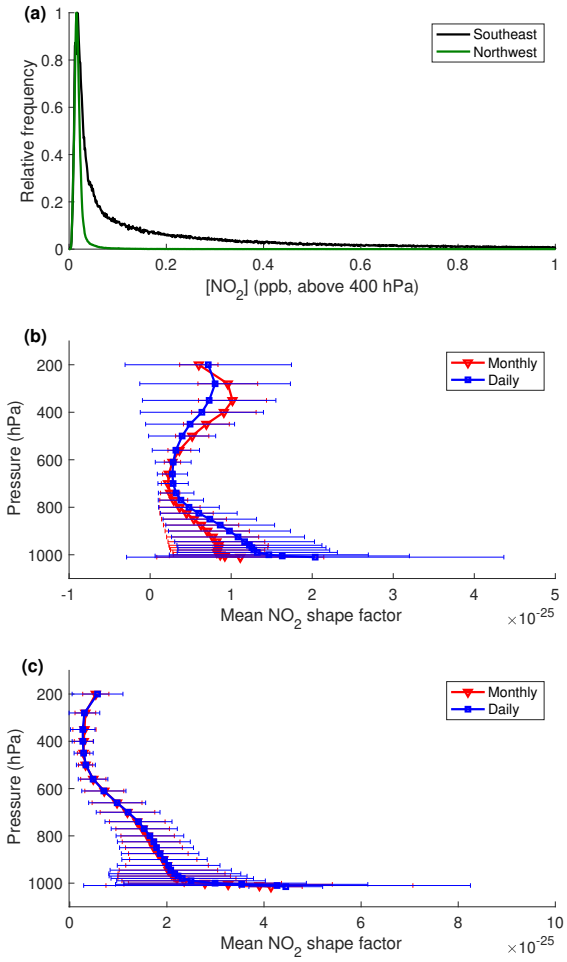

Figure R3: **(a)** Frequency distribution (normalized to maximum) of average NO_2 above 400 hPa in the a priori profiles for the southeast and northwest US, from Jun–Aug 2012. **(b–c)** Mean a priori NO_2 shape factors over the southeast US (b) and northwest US (c) for Jun–Aug, 2012. Shape factors are defined as the NO_2 profile in mixing ratio divided by its integral in molec cm^{-2}. The error bars are $\pm 1\sigma$. The regions (SE and NW US) are shown in Fig. S4.

systematically greater AMFs (and therefore smaller VCDs) in the southeast when using the monthly profiles if the scattering weights ($w(p)$ in Eq. 2) are greater in the UT than near the surface, which is usually the case. In contrast, Fig. R3c shows no difference in the monthly or daily shape factors for the northwest US. For interested readers, a more mathematical argument is given in Sect. S2 of the supplement.

The implication is that, for regions with long-tailed statistical distributions of NO_2 concentrations, there will be systematic differences between a product using monthly average and daily a priori profiles. It is likely that the VCDs calculated using the daily a priori profiles are more accurate, because in theory daily a priori profiles should properly account for that long tail on days when it is relevant, whereas monthly profiles will average in the extreme values.

Finally we note that this difference between daily and monthly profiles may change in the future. Laughner et al. (2018) found that the simulation providing the NO_2 profiles had too much lightning in the southeast US. Correcting that may reduce the skewness of the UT NO_2 distribution. Work is underway to improve the representation of lightning for the southeast US NO_2 profiles. "

page17line5 Is there probably a name or reference to this temperature profile?
Added citation to Bucsela et al. (2006)

page18line6-13 There are introductions of the previous method and why PSM method cannot be used here. It might be better to add a small introduction of the new CVM which is actually used in this study.
The concept of the old and new CVM methods are the same, only the implementation differs. We have clarified this:

"BEHR v3.0A also uses a CVM gridding algorithm, however the implementation was changed. The new CVM algorithm is a slightly modified version of that provided by Kuhlmann et al. (2014), with a custom interface to allow communication between the Python code from `https://github.com/gkuhl/omi` and the BEHR Matlab code."

page19line7 The ocean reflectance is calculated without MODIS data, therefore I do not understand the goal of this change to 460 nm. Even the impact is small, the re- flectance at 430 nm shall be used because of the reason exactly described in the text.
This could be argued either way; using the 430 nm reflectance would be more representative of the NO_2 fitting window, but using the 460 nm reflectance is consistent with the land reflectance wavelength, meaning that whatever small bias is imposed by using a wavelength on the edge of the NO_2 fitting window is consistent between the land and ocean. We have explained this more in the text:

"In v3.0B, this was changed to be 460 nm, which is within the MODIS band used (459–479 nm). **While both approaches have merit, we chose to**

move towards calculating the surface reflectance at similar wavelengths for consistency between the ocean and land data. The change in VCD retrieved over ocean is very small..."

References

Acarreta, J. R., De Haan, J. F., and Stammes, P.: Cloud pressure retrieval using the O2-O2 absorption band at 477 nm, J. Geophys. Res. Atmos., 109, D05 204, doi:10.1029/2003JD003915, URL http://dx.doi.org/10.1029/2003JD003915, 2004.

Boersma, K. F., Vinken, G. C. M., and Eskes, H. J.: Representativeness errors in comparing chemistry transport and chemistry climate models with satellite UV–Vis tropospheric column retrievals, Geosci. Model Dev., 9, 875–898, doi:10.5194/gmd-9-875-2016, URL https://doi.org/10.5194/gmd-9-875-2016, 2016.

Bucsela, E., Celarier, E., Wenig, M., Gleason, J., Veefkind, J., Boersma, K., and Brinksma, E.: Algorithm for NO_2 vertical column retrieval from the ozone monitoring instrument, IEEE Trans. Geosci. Remote Sens., 44, 1245–1258, doi:10.1109/tgrs.2005.863715, URL https://doi.org/10.1109/tgrs.2005.863715, 2006.

Burrows, J. P. and Chance, K. V.: SCIAMACHY and GOME: the scientific objectives, in: Proc. SPIE, vol. 1715, doi:10.1117/12.140201, 1993.

Burrows, J. P., Richter, A., Dehn, A., Deters, B., Himmelmann, S., Voigt, S., and Orphal, J.: Atmospheric remote-sensing reference data from GOME–2. Temperature-dependent absorption cross section of O_3 in the 231-794 nm range, J. Quant. Spectrosc. Radiat. Transfer, 61, 509–517, 1999a.

Burrows, J. P., Weber, M., Buchwitz, M., Rozanov, V., Ladstätter-Weißenmayer, A., Richter, A., DeBeek, R., Hoogen, R., Bramstedt, K., Eichmann, K.-U., and Eisinger, M.: The Global Ozone Monitoring Experiment (GOME): Mission Concept and First Scientific Results, J. Atmos. Sci., 56, 151–175, doi:10.1175/1520-0469(1999)056⟨0151:TGOMEG⟩2.0.CO;2, 1999b.

Cahalan, R. F., Ridgway, W., Wiscombe, W. J., Gollmer, S., and Harshvardhan: Independent Pixel and Monte Carlo Estimates of Stratocumulus Albedo, J. Atmos. Sci., 51, 3776–3790, doi:10.1175/1520-0469(1994)051⟨3776:ipamce⟩2.0.co;2, URL https://doi.org/10.1175/1520-0469(1994)051<3776:ipamce>2.0.co;2, 1994.

Choi, S., Joiner, J., Choi, Y., Duncan, B. N., Vasilkov, A., Krotkov, N., and Bucsela, E.: First estimates of global free-tropospheric NO_2 abundances derived using a cloud-slicing technique applied to satellite observations from the Aura Ozone Monitoring Instrument (OMI), Atmos. Chem. Phys., 14, 10 565–10 588, doi:10.5194/acp-14-10565-2014, URL http://www.atmos-chem-phys.net/14/10565/2014/, 2014.

Emmons, L. K., Walters, S., Hess, P. G., Lamarque, J.-F., Pfister, G. G., Fillmore, D., Granier, C., Guenther, A., Kinnison, D., Laepple, T., Orlando, J., Tie, X., Tyndall, G.,

Wiedinmyer, C., Baughcum, S. L., and Kloster, S.: Description and evaluation of the Model for Ozone and Related chemical Tracers, version 4 (MOZART-4), Geosci. Model Dev., 3, 43–67, doi:10.5194/gmd-3-43-2010, URL http://www.geosci-model-dev.net/3/43/2010/, 2010.

Gorshelev, V., Serdyuchenko, A., Weber, M., Chehade, W., and Burrows, J. P.: High spectral resolution ozone absorption cross-sections—Part 1: Measurements, data analysis and comparison with previous measurements around 293 K, Atmos. Meas. Tech., 7, 609–624, doi:10.5194/amt-7-609-2014, URL https://www.atmos-meas-tech.net/7/609/2014/, 2014.

Jiang, Z., McDonald, B. C., Worden, H., Worden, J. R., Miyazaki, K., Qu, Z., Henze, D. K., Jones, D. B. A., Arellano, A. F., Fischer, E. V., Zhu, L., and Boersma, K. F.: Unexpected slowdown of US pollutant emission reduction in the past decade, PNAS, 115, 5099–5104, doi:10.1073/pnas.1801191115, URL https://doi.org/10.1073/pnas.1801191115, 2018.

Jin, Z., Charlock, T. P., Smith, W. L., and Rutledge, K.: A parameterization of ocean surface albedo, Geophys, Res, Lett,, 31, L22 301, doi:10.1029/2004GL021180, URL http://dx.doi.org/10.1029/2004GL021180, 2004.

Jin, Z., Charlock, T., Rutledge, K., Stamnes, K., and Wang, Y.: Analytical solution of radiative transfer in the coupled atmosphere-ocean system with a rough surface, Appl. Opt., 45, 7443–7455, 2006.

Kuhlmann, G., Hartl, A., Cheung, H. M., Lam, Y. F., and Wenig, M. O.: A novel gridding algorithm to create regional trace gas maps from satellite observations, Atmos. Meas. Tech., 7, 451–467, doi:10.5194/amt-7-451-2014, URL https://www.atmos-meas-tech.net/7/451/2014/, 2014.

Lamsal, L. N., Martin, R. V., van Donkelaar, A., Steinbacher, M., Celarier, E. A., Bucsela, E., Dunlea, E. J., and Pinto, J. P.: Ground-level nitrogen dioxide concentrations inferred from the satellite-borne Ozone Monitoring Instrument, J. Geophys. Res. Atmos., 113, D16 308, doi:10.1029/2007JD009235, URL https://agupubs.onlinelibrary.wiley.com/doi/abs/10.1029/2007JD009235, 2008.

Laughner, J. L., Zare, A., and Cohen, R. C.: Effects of daily meteorology on the interpretation of space-based remote sensing of NO_2, Atmos. Chem. Phys., 16, 15 247–15 264, doi:10.5194/acp-16-15247-2016, URL http://www.atmos-chem-phys.net/16/15247/2016/, 2016.

Laughner, J. L., Zhu, Q., and Cohen, R.: Evaluation of version 3.0B of the BEHR OMI NO_2 product, Atmos. Meas. Tech. Discuss., 2018, 1–25, doi:10.5194/amt-2018-248, URL https://www.atmos-meas-tech-discuss.net/amt-2018-248/, 2018.

Marais, E. A., Jacob, D. J., Choi, S., Joiner, J., Belmonte-Rivas, M., Cohen, R. C., Beirle, S., Murray, L. T., Schiferl, L., Shah, V., and Jaeglé, L.: Nitrogen oxides in the global upper troposphere: interpreting cloud-sliced NO_2 observations from the OMI satellite instrument, Atmos. Chem. Phys. Discuss., 2018, 1–14, doi:10.5194/acp-2018-556, URL https://www.atmos-chem-phys-discuss.net/acp-2018-556/, 2018.

Marshak, A., Davis, A., Cahalan, R., and Wiscombe, W.: Nonlocal independent pixel approximation: direct and inverse problems, IEEE Trans. Geosci. Rem. Sens., 36, 192–205, doi:10.1109/36.655329, URL https://doi.org/10.1109/36.655329, 1998.

Noel, S., Bovensmann, H., Burrows, J. P., Frerick, J., Chance, K. V., Goede, A. P. H., and Muller, C.: SCIAMACHY instrument on ENVISAT-1, in: Sensors, Systems, and Next-Generation Satellites II, edited by Fujisada, H., SPIE, doi:10.1117/12.333621, URL https://doi.org/10.1117/12.333621, 1998.

Pickering, K. E., Bucsela, E., Allen, D., Ring, A., Holzworth, R., and Krotkov, N.: Estimates of lightning NO_x production based on OMI NO2 observations over the Gulf of Mexico, J. Geophys. Res. Atmos., 121, 8668–8691, doi:10.1002/2015JD024179, URL http://dx.doi.org/10.1002/2015JD024179, 2015JD024179, 2016.

Platnick, S., King, M., Wind, G., Ackerman, S., Menzel, P., and Frey, R.: MODIS/Aqua Clouds 5-Min L2 Swath 1km and 5km. NASA MODIS Adaptive Processing System, Goddard Space Flight Center, USA, doi:10.5067/MODIS/MYD06_L2.006, 2015.

Russell, A., Perring, A., Valin, L., Bucsela, E., Browne, E., Min, K., Wooldridge, P., and Cohen, R.: "A high spatial resolution retrieval of NO_2 column densities from OMI: method and evalutation", Atmos. Chem. Phys., 11, 8543–8554, doi:10.5194/acp-11-8543-2011, 2011.

Russell, A. R., Valin, L. C., and Cohen, R. C.: Trends in OMI NO_2 observations over the United States: effects of emission control technology and the economic recession, Atmos. Chem. Phys., 12, 12 197–12 209, doi:10.5194/acp-12-12197-2012, 2012.

Ziemke, J., Chandra, S., and Bhartia, P.: Cloud slicing: A new technique to derive upper tropospheric ozone from satellite measurements, J. Geophys. Res. Atmos., 106, 9853–9867, 2001.